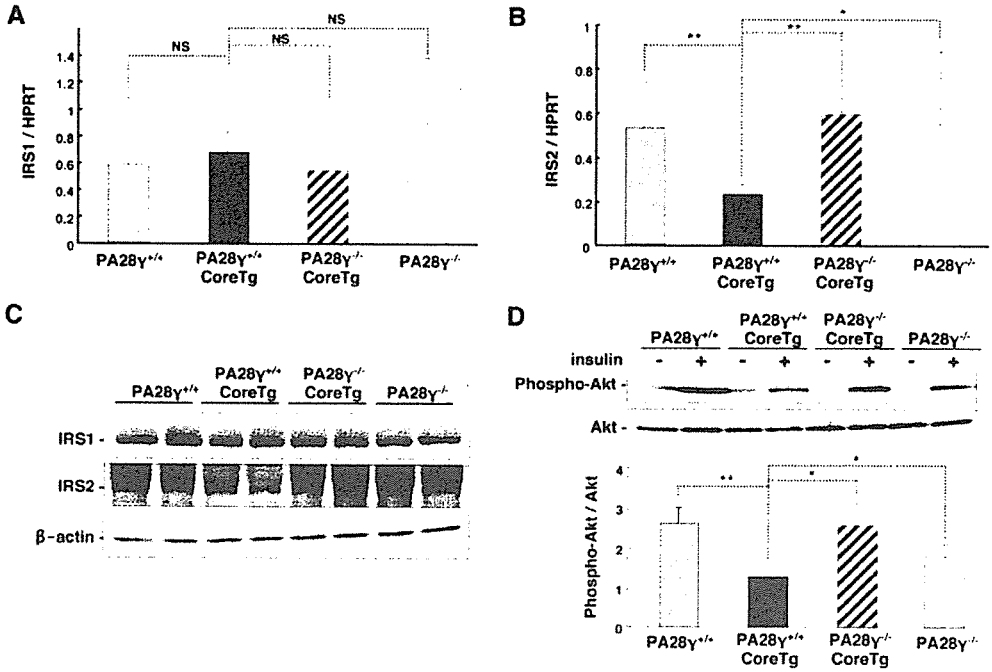

FIG. 6. PA28γ participated in the inhibition of the IRS2 expression and Akt phosphorylation induced by HCV core protein. The transcription of IRS1 (A) and IRS2 (B) was estimated by quantitative RT-PCR ($n = 5$ in each group). (C) The expression levels of IRS1 and IRS2 in the livers of the mice were determined by immunoblotting with specific antibodies. (D) Phosphorylation of Akt in the livers of the mice was examined by immunoblotting with antibodies against Akt and phosphorylated Akt. The ratio of Akt phosphorylation was determined by computer software based on the densities of phosphorylated Akt and a total amount of Akt ($n = 3$ in each group). The data presented are representative of three independent experiments. $*P < 0.05$; $**P < 0.01$. NS, not statistically significant; HPRT, hypoxanthine phosphoribosyl transferase.

ous study, the reduction in the plasma glucose concentration after insulin administration was impaired in PA28γ$^{+/+}$CoreTg mice (47). In this study, PA28γ$^{-/-}$CoreTg mice exhibited a normal insulin level comparable to those of PA28γ$^{+/+}$ and PA28γ$^{-/-}$ mice by an insulin tolerance test, in contrast to PA28γ$^{+/+}$CoreTg mice, in which a high concentration of plasma glucose was detected at all time points, as previously reported (Fig. 3B). These data suggest that hyperinsulinemia was induced in PA28γ$^{+/+}$CoreTg mice to compensate for insulin resistance and retain a physiological level of plasma glucose and that PA28γ participates in the development of hyperinsulinemia and insulin resistance in PA28γ$^{+/+}$CoreTg mice.

Morphology of pancreatic islets. Hyperinsulinemia and insulin resistance are expected to enlarge the pancreatic islet mass due to the overexpression of insulin. Our previous report showed the enlargement of the pancreatic islets in PA28γ$^{+/+}$ CoreTg mice. To clarify whether a knockout of the PA28γ gene restores the enlarged pancreatic islets to their normal size, the morphology of the pancreatic islets of the mice was evaluated by histologic examination (Fig. 4A). The relative islet area in the pancreatic cells of the PA28γ$^{-/-}$CoreTg mice was smaller than that of PA28γ$^{+/+}$CoreTg mice and comparable to that of PA28γ$^{+/+}$ and PA28γ$^{-/-}$ mice (Fig. 4B). Infiltration of inflammatory cells within or surrounding the islets was not found in all genotypes of mice. These results suggest that PA28γ also participates in the enlargement of pancreatic islets induced in PA28γ$^{+/+}$CoreTg mice.

PA28γ impairs the insulin-signaling pathway through the suppression of both tyrosine phosphorylation of IRS1 and expression of IRS2. Insulin binds to insulin receptors, resulting in the activation of downstream signaling (26). The activated insulin receptors phosphorylate themselves, IRS1, and IRS2. Phosphorylated IRS1 and IRS2 can activate phosphatidylinositol 3 (PI3)-kinase signaling, leading to the activation of glucose metabolism and cell growth. Our previous report showed that tyrosine phosphorylation of IRS1 is suppressed in the livers of PA28γ$^{+/+}$CoreTg mice and that the administration of anti-TNF-α antibody restores insulin sensitivity (47). We examined whether a knockout of the PA28γ gene could restore the tyrosine phosphorylation of IRS1. Tyrosine phosphorylation of IRS1 was suppressed in the livers of PA28γ$^{+/+}$ CoreTg mice in response to insulin stimulation, whereas it was recovered in PA28γ$^{-/-}$CoreTg mice to levels comparable to those in PA28γ$^{+/+}$and PA28γ$^{-/-}$ mice (Fig. 5).

Chronic hyperinsulinemia downregulates the expression of IRS2, which is one of the essential components of the insulin-signaling pathway in the liver (46). However, in our previous study, we showed that there was no significant difference in the phosphorylation of IRS2 between PA28γ$^{+/+}$CoreTg mice and their normal littermates (47). To gain more insight into the mechanisms of regulation of IRS expression, we determined the transcription and translation of IRS1 and IRS2 in the livers of the mice by real-time PCR and Western blotting, respectively. Although there was no significant difference in IRS1 expression at either the transcriptional or translational level among the mice

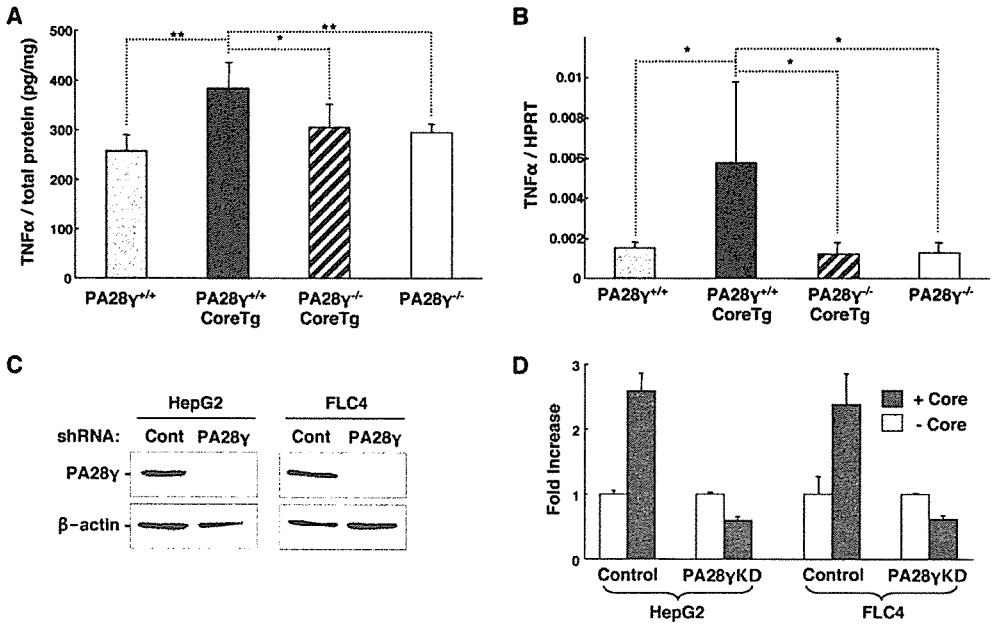

FIG. 7. PA28γ was required for activation of the TNF-α promoter by the HCV core protein. (A) Expression of TNF-α in the livers of mice was determined by ELISA (n = 5 in each group). (B) TNF-α mRNA in the livers of mice was examined by quantitative RT-PCR (n = 5 in each group). (C) Knockdown of the expression of PA28γ in the HepG2 and FLC-4 cell lines by the introduction of a plasmid encoding a short hairpin RNA (shRNA) targeted to the PA28γ gene. The expression levels of PA28γ and β-actin were determined by immunoblotting with specific antibodies. (D) Promoter activity of TNF-α in the presence or absence of the HCV core protein was determined by luciferase assay in the PA28γ-knockdown and control cell lines. The data presented are representative of three independent experiments. HPRT, hypoxanthine phosphoribosyl transferase.

(Fig. 6A and C), the expression of IRS2 was clearly impaired in PA28γ$^{+/+}$CoreTg mice at both the transcriptional and translational levels compared with that in other mice (Fig. 6B and C). The serine/threonine protein kinase Akt is phosphorylated by phosphoinositide-dependent kinase 1 (PDK1) under the activated condition of IRS family proteins (26). The insulin-induced phosphorylation of Akt was suppressed in the livers of PA28γ$^{+/+}$ CoreTg mice but not in those of PA28γ$^{+/+}$, PA28γ$^{-/-}$, or PA28γ$^{-/-}$CoreTg mice (Fig. 6D). These results suggest that the expression of the HCV core protein in the livers of mice in the presence of PA28γ impairs the insulin-signaling pathway through the suppression of both the tyrosine phosphorylation of IRS1 and the expression of IRS2.

PA28γ is required for activation of the TNF-α promoter by HCV core protein. TNF-α is an adipokine (54) and suppresses the signaling pathway of IRS1 and IRS2 (14, 42). Several reports suggested that the serum TNF-α level is higher in HCV patients than in healthy individuals (19, 37). Elevations of TNF-α levels have also been demonstrated in the livers of PA28γ$^{+/+}$CoreTg mice (47). To determine the involvement of PA28γ in the enhancement of TNF-α expression, the expression of TNF-α in the livers of each genotype was determined by ELISA and real-time PCR (Fig. 7A and B). Transcription and translation of TNF-α were increased in the livers of PA28γ$^{+/+}$ CoreTg mice but were restored in the livers of PA28γ$^{-/-}$ CoreTg mice to levels comparable to those of PA28γ$^{+/+}$ and PA28γ$^{-/-}$ mice. To determine the effect of PA28γ expression on the promoter activity of TNF-α in human liver cells, PA28γ-knockdown human hepatoma cell lines HepG2 and FLC4 were established by the introduction of a plasmid encoding a short hairpin RNA targeting the PA28γ gene in the cell lines. The expression of PA28γ was clearly suppressed in the cell lines (Fig. 7C). The expression of HCV core protein in the hepatoma cell lines potentiated TNF-α promoter activity, whereas the promoter activation by the HCV core protein was suppressed in the PA28γ-knockdown cell lines (Fig. 7D). These results suggest that PA28γ is required for the activation of the TNF-α promoter induced by the expression of the HCV core protein in human hepatoma cell lines.

DISCUSSION

HCV infection has a close association with type 2 diabetes, which is a polygenic disease with a pathophysiology that includes a defect in insulin secretion, increased hepatic glucose production, and resistance to the action of insulin (2, 8, 18). Insulin binds to insulin receptors, which exhibit tyrosine kinase activity, leading to the autophosphorylation and phosphorylation of IRS (56). Tyrosine phosphorylation in IRS proteins leads to the interaction between IRS proteins and the regulatory subunit p85 of PI3-kinase, which enhances glucose uptake and inhibits lypolysis (21). Activated PI3-kinase phosphorylates phosphatidylinositol 4,5-biphosphate to produce phosphatidylinositol 3,4,5-triphosphate, which contributes to the activation of PDK1 (55). Activated PDK1 phosphorylates downstream substrates including Akt and other kinases (55). A diabetic phenotype that included insulin resistance was found in IRS2-knockout mice with normal growth (57), although a

knockout of the IRS1 gene has been shown to lead to growth retardation and insulin resistance but not overt diabetes (5, 52). The double knockdown of IRS1 and IRS2 genes in the liver induces hyperinsulinemia and insulin resistance in mice (53). The reduction of both IRS1 and IRS2 under conditions of insulin resistance and hyperinsulinemia (3) and in the livers of *ob/ob* mice, an obese diabetic mouse model (20), has been reported previously. In the present study, the expression of the HCV core protein reduced the phosphorylation of tyrosine on IRS1 and the production of IRS2 in the livers of mice but did not completely abolish the activities of these genes, suggesting that residual activities of IRS transfer a faint signal to the downstream region of IRS. Therefore, PA28γ$^{+/+}$CoreTg mice may exhibit a milder phenotype than IRS1- and/or IRS2-knockout mice. In this study, knockout of the PA28γ gene restored the insulin sensitivity and signaling of IRS1 and IRS2 in PA28γ$^{+/+}$CoreTg mice, suggesting that the expression of the HCV core protein leads to the dysfunction of both IRS1 and IRS2 through a PA28γ-dependent pathway.

Our previous study suggested that the induction of TNF-α by the HCV core protein plays a role in insulin resistance (47). An increase in TNF-α levels has been correlated with obesity and insulin resistance in animal models and humans (14, 42). However, the mechanism by which TNF-α induces insulin resistance is not completely known. The expression of TNF-α has been shown to be increased in PA28γ$^{+/+}$CoreTg mice, resulting in the suppression of phosphorylation of IRS1, and insulin sensitivity in PA28γ$^{+/+}$CoreTg was improved by the administration of an anti-TNF-α antibody (47). In the present study, the expression level of TNF-α in PA28γ$^{-/-}$CoreTg mice was similar to that in PA28γ$^{-/-}$ mice or their normal littermates. The expression of the HCV core protein enhanced the promoter activity of the TNF-α gene in human liver cell lines but not in those with a knockdown of the PA28γ gene by RNA interference (Fig. 7D). These data suggest that PA28γ plays a crucial role in HCV core-induced expression of TNF-α. Sterol regulatory element-binding proteins (SREBPs) were shown to be increased at the stage of viremia in HCV-infected chimpanzees (49). SREBPs are known to regulate not only the biosynthesis of lipid but also the transcription of IRS2 and TNF-α (17, 45). Therefore, it might be feasible to speculate that the HCV core protein may cooperate with PA28γ to regulate the expression of SREBPs.

Houstis et al. previously reported that reactive oxygen species (ROS) are increased in both cellular and mouse models of insulin resistance induced by treatment with TNF-α or dexamethasone and that insulin sensitivity was restored by treatment with small antioxidant molecules (16). The HCV core protein potentiates ROS production in hepatoma cells and HCV core gene-transgenic mice (23, 34, 41). Accelerated production of ROS results in mitochondrion dysfunction, which contributes to a decrease in fatty acid oxidation. Defects in mitochondrial fatty acid oxidation enhance the production of intracellular fatty acyl coenzyme A (CoA) and diacylglycerol (48, 58). Mitochondrion dysfunction and accumulation of lipid droplets in mice expressing the HCV core or the full-length HCV polyprotein have been reported (27, 34). An increase in lipid droplets also leads to the accumulation of fatty acid CoA and diacylglycerol (48, 58). Fatty acyl CoA and diacylglycerol nonspecifically activate the Ser/Thr kinase cascade, leading to the enhancement of the serine phosphorylation of IRS1 (26). Serine phosphorylation on IRS1 blocks the tyrosine phosphorylation of IRS1 by insulin receptors (26). In the present study, however, serine phosphorylation of IRS1 in PA28γ$^{+/+}$ CoreTg mice was similar to that in PA28γ$^{-/-}$CoreTg mice (data not shown). TNF-α signaling pathways other than the accumulation of ROS and fatty acid intermediates may also participate in the inhibition of tyrosine phosphorylation on IRS1 in PA28γ$^{+/+}$ CoreTg mice.

How does the HCV core protein induce TNF-α production? Our previous report suggests that the HCV core protein is degraded through a PA28γ-dependent pathway (32). Recently, PA28γ has been shown to participate in the proteasome-dependent degradation of steroid receptor coactivator 3 (28). Degradation products of the HCV core protein via the PA28γ-dependent pathway may regulate the promoter activity of the TNF-α gene. PA28 proteins are necessary and sufficient to fully reconstitute Hsp90-initiated refolding together with Hsc70 and Hsp40 (31). Therefore, it might also be feasible to speculate that the HCV core protein refolded by an Hsp90/PA28γ-dependent pathway activates the promoter of the TNF-α gene together with an unknown transcription factor(s) or regulator(s).

In conclusion, the data obtained in this study suggest that the expression of the HCV core protein enhances the production of TNF-α and suppresses the phosphorylation of tyrosine on IRS1 and the production of IRS2 through a PA28γ-dependent pathway, thereby leading to insulin resistance. PA28γ may be a novel target for the treatment of HCV-induced diabetes.

ACKNOWLEDGMENTS

We gratefully thank H. Murase for secretarial work.

This study was supported in part by grants-in-aid from the Ministry of Health, Labor, and Welfare; the Ministry of Education, Culture, Sports, Science, and Technology; the Program for the Promotion of Fundamental Studies in Health Sciences of the National Institute of Biomedical Innovation (NIBIO); the 21st Century Center of Excellence Program; and the Foundation for Biomedical Research and Innovation.

REFERENCES

1. **Aizaki, H., Y. Aoki, T. Harada, K. Ishii, T. Suzuki, S. Nagamori, G. Toda, Y. Matsuura, and T. Miyamura.** 1998. Full-length complementary DNA of hepatitis C virus genome from an infectious blood sample. Hepatology **27:** 621–627.
2. **Allison, M. E., T. Wreghitt, C. R. Palmer, and G. J. Alexander.** 1994. Evidence for a link between hepatitis C virus infection and diabetes mellitus in a cirrhotic population. J. Hepatol. **21:**1135–1139.
3. **Anai, M., M. Funaki, T. Ogihara, J. Terasaki, K. Inukai, H. Katagiri, Y. Fukushima, Y. Yazaki, M. Kikuchi, Y. Oka, and T. Asano.** 1998. Altered expression levels and impaired steps in the pathway to phosphatidylinositol 3-kinase activation via insulin receptor substrates 1 and 2 in Zucker fatty rats. Diabetes **47:**13–23.
4. **Aoyagi, K., C. Ohue, K. Iida, T. Kimura, E. Tanaka, K. Kiyosawa, and S. Yagi.** 1999. Development of a simple and highly sensitive enzyme immunoassay for hepatitis C virus core antigen. J. Clin. Microbiol. **37:**1802–1808.
5. **Araki, E., M. A. Lipes, M. E. Patti, J. C. Bruning, B. Haag III, R. S. Johnson, and C. R. Kahn.** 1994. Alternative pathway of insulin signalling in mice with targeted disruption of the IRS-1 gene. Nature **372:**186–190.
6. **Bukh, J., R. H. Purcell, and R. H. Miller.** 1994. Sequence analysis of the core gene of 14 hepatitis C virus genotypes. Proc. Natl. Acad. Sci. USA **91:**8239–8243.
7. **Caronia, S., K. Taylor, L. Pagliaro, C. Carr, U. Palazzo, J. Petrik, S. O'Rahilly, S. Shore, B. D. Tom, and G. J. Alexander.** 1999. Further evidence for an association between non-insulin-dependent diabetes mellitus and chronic hepatitis C virus infection. Hepatology **30:**1059–1063.
8. **Cavaghan, M. K., D. A. Ehrmann, and K. S. Polonsky.** 2000. Interactions between insulin resistance and insulin secretion in the development of glucose intolerance. J. Clin. Investig. **106:**329–333.
9. **Choo, Q. L., G. Kuo, A. J. Weiner, L. R. Overby, D. W. Bradley, and M. Houghton.** 1989. Isolation of a cDNA clone derived from a blood-borne non-A, non-B viral hepatitis genome. Science **244:**359–362.

10. **Choo, Q. L., K. H. Richman, J. H. Han, K. Berger, C. Lee, C. Dong, C. Gallegos, D. Coit, R. Medina-Selby, P. J. Barr, et al.** 1991. Genetic organization and diversity of the hepatitis C virus. Proc. Natl. Acad. Sci. USA **88**:2451–2455.
11. **Falcon, V., N. Acosta-Rivero, G. Chinea, J. Gavilondo, M. C. de la Rosa, I. Menendez, S. Duenas-Carrera, A. Vina, W. Garcia, B. Gra, M. Noa, E. Reytor, M. T. Barcelo, F. Alvarez, and J. Morales-Grillo.** 2003. Ultrastructural evidences of HCV infection in hepatocytes of chronically HCV-infected patients. Biochem. Biophys. Res. Commun. **305**:1085–1090.
12. **Grakoui, A., D. W. McCourt, C. Wychowski, S. M. Feinstone, and C. M. Rice.** 1993. Characterization of the hepatitis C virus-encoded serine proteinase: determination of proteinase-dependent polyprotein cleavage sites. J. Virol. **67**:2832–2843.
13. **Gumber, S. C., and S. Chopra.** 1995. Hepatitis C: a multifaceted disease. Review of extrahepatic manifestations. Ann. Intern. Med. **123**:615–620.
14. **Hotamisligil, G. S.** 1999. The role of TNFalpha and TNF receptors in obesity and insulin resistance. J. Intern. Med. **245**:621–625.
15. **Houghton, M., A. Weiner, J. Han, G. Kuo, and Q. L. Choo.** 1991. Molecular biology of the hepatitis C viruses: implications for diagnosis, development and control of viral disease. Hepatology **14**:381–388.
16. **Houstis, N., E. D. Rosen, and E. S. Lander.** 2006. Reactive oxygen species have a causal role in multiple forms of insulin resistance. Nature **440**:944–948.
17. **Ide, T., H. Shimano, N. Yahagi, T. Matsuzaka, M. Nakakuki, T. Yamamoto, Y. Nakagawa, A. Takahashi, H. Suzuki, H. Sone, H. Toyoshima, A. Fukamizu, and N. Yamada.** 2004. SREBPs suppress IRS-2-mediated insulin signalling in the liver. Nat. Cell Biol. **6**:351–357.
18. **Kahn, B. B.** 1998. Type 2 diabetes: when insulin secretion fails to compensate for insulin resistance. Cell **92**:593–596.
19. **Kallinowski, B., K. Haseroth, G. Marinos, C. Hanck, W. Stremmel, L. Theilmann, M. V. Singer, and S. Rossol.** 1998. Induction of tumour necrosis factor (TNF) receptor type p55 and p75 in patients with chronic hepatitis C virus (HCV) infection. Clin. Exp. Immunol. **111**:269–277.
20. **Kerouz, N. J., D. Horsch, S. Pons, and C. R. Kahn.** 1997. Differential regulation of insulin receptor substrates-1 and -2 (IRS-1 and IRS-2) and phosphatidylinositol 3-kinase isoforms in liver and muscle of the obese diabetic (ob/ob) mouse. J. Clin. Investig. **100**:3164–3172.
21. **Kido, Y., J. Nakae, and D. Accili.** 2001. Clinical review 125: the insulin receptor and its cellular targets. J. Clin. Endocrinol. Metab. **86**:972–979.
22. **Kiyosawa, K., T. Sodeyama, E. Tanaka, Y. Gibo, K. Yoshizawa, Y. Nakano, S. Furuta, Y. Akahane, K. Nishioka, R. H. Purcell, et al.** 1990. Interrelationship of blood transfusion, non-A, non-B hepatitis and hepatocellular carcinoma: analysis by detection of antibody to hepatitis C virus. Hepatology **12**:671–675.
23. **Korenaga, M., T. Wang, Y. Li, L. A. Showalter, T. Chan, J. Sun, and S. A. Weinman.** 2005. Hepatitis C virus core protein inhibits mitochondrial electron transport and increases reactive oxygen species (ROS) production. J. Biol. Chem. **280**:37481–37488.
24. **Kuo, G., Q. L. Choo, H. J. Alter, G. L. Gitnick, A. G. Redeker, R. H. Purcell, T. Miyamura, J. L. Dienstag, M. J. Alter, C. E. Stevens, et al.** 1989. An assay for circulating antibodies to a major etiologic virus of human non-A, non-B hepatitis. Science **244**:362–364.
25. **Kuprash, D. V., I. A. Udalova, R. L. Turetskaya, D. Kwiatkowski, N. R. Rice, and S. A. Nedospasov.** 1999. Similarities and differences between human and murine TNF promoters in their response to lipopolysaccharide. J. Immunol. **162**:4045–4052.
26. **Lazar, D. F., and A. R. Saltiel.** 2006. Lipid phosphatases as drug discovery targets for type 2 diabetes. Nat. Rev. Drug Discov. **5**:333–342.
27. **Lerat, H., M. Honda, M. R. Beard, K. Loesch, J. Sun, Y. Yang, M. Okuda, R. Gosert, S. Y. Xiao, S. A. Weinman, and S. M. Lemon.** 2002. Steatosis and liver cancer in transgenic mice expressing the structural and nonstructural proteins of hepatitis C virus. Gastroenterology **122**:352–365.
28. **Li, X., D. M. Lonard, S. Y. Jung, A. Malovannaya, Q. Feng, J. Qin, S. Y. Tsai, M. J. Tsai, and B. W. O'Malley.** 2006. The SRC-3/AIB1 coactivator is degraded in a ubiquitin- and ATP-independent manner by the REGgamma proteasome. Cell **124**:381–392.
29. **Mason, A. L., J. Y. Lau, N. Hoang, K. Qian, G. J. Alexander, L. Xu, L. Guo, S. Jacob, F. G. Regenstein, R. Zimmerman, J. E. Everhart, C. Wasserfall, N. K. Maclaren, and R. P. Perrillo.** 1999. Association of diabetes mellitus and chronic hepatitis C virus infection. Hepatology **29**:328–333.
30. **McLauchlan, J., M. K. Lemberg, G. Hope, and B. Martoglio.** 2002. Intramembrane proteolysis promotes trafficking of hepatitis C virus core protein to lipid droplets. EMBO J. **21**:3980–3988.
31. **Minami, Y., H. Kawasaki, M. Minami, N. Tanahashi, K. Tanaka, and I. Yahara.** 2000. A critical role for the proteasome activator PA28 in the Hsp90-dependent protein refolding. J. Biol. Chem. **275**:9055–9061.
32. **Moriishi, K., T. Okabayashi, K. Nakai, K. Moriya, K. Koike, S. Murata, T. Chiba, K. Tanaka, R. Suzuki, T. Suzuki, T. Miyamura, and Y. Matsuura.** 2003. Proteasome activator PA28γ-dependent nuclear retention and degradation of hepatitis C virus core protein. J. Virol. **77**:10237–10249.
33. **Moriya, K., H. Fujie, Y. Shintani, H. Yotsuyanagi, T. Tsutsumi, K. Ishibashi, Y. Matsuura, S. Kimura, T. Miyamura, and K. Koike.** 1998. The core protein of hepatitis C virus induces hepatocellular carcinoma in transgenic mice. Nat. Med. **4**:1065–1067.
34. **Moriya, K., K. Nakagawa, T. Santa, Y. Shintani, H. Fujie, H. Miyoshi, T. Tsutsumi, T. Miyazawa, K. Ishibashi, T. Horie, K. Imai, T. Todoroki, S. Kimura, and K. Koike.** 2001. Oxidative stress in the absence of inflammation in a mouse model for hepatitis C virus-associated hepatocarcinogenesis. Cancer Res. **61**:4365–4370.
35. **Moriya, K., H. Yotsuyanagi, Y. Shintani, H. Fujie, K. Ishibashi, Y. Matsuura, T. Miyamura, and K. Koike.** 1997. Hepatitis C virus core protein induces hepatic steatosis in transgenic mice. J Gen. Virol. **78**:1527–1531.
36. **Murata, S., H. Kawahara, S. Tohma, K. Yamamoto, M. Kasahara, Y. Nabeshima, K. Tanaka, and T. Chiba.** 1999. Growth retardation in mice lacking the proteasome activator PA28gamma. J. Biol. Chem. **274**:38211–38215.
37. **Nelson, D. R., H. L. Lim, C. G. Marousis, J. W. Fang, G. L. Davis, L. Shen, M. S. Urdea, J. A. Kolberg, and J. Y. Lau.** 1997. Activation of tumor necrosis factor-alpha system in chronic hepatitis C virus infection. Dig. Dis. Sci. **42**:2487–2494.
38. **Niwa, H., K. Yamamura, and J. Miyazaki.** 1991. Efficient selection for high-expression transfectants with a novel eukaryotic vector. Gene **108**:193–199.
39. **Ogino, T., H. Fukuda, S. Imajoh-Ohmi, M. Kohara, and A. Nomoto.** 2004. Membrane binding properties and terminal residues of the mature hepatitis C virus capsid protein in insect cells. J. Virol. **78**:11766–11777.
40. **Okamoto, K., K. Moriishi, T. Miyamura, and Y. Matsuura.** 2004. Intramembrane proteolysis and endoplasmic reticulum retention of hepatitis C virus core protein. J. Virol. **78**:6370–6380.
41. **Okuda, M., K. Li, M. R. Beard, L. A. Showalter, F. Scholle, S. M. Lemon, and S. A. Weinman.** 2002. Mitochondrial injury, oxidative stress, and antioxidant gene expression are induced by hepatitis C virus core protein. Gastroenterology **122**:366–375.
42. **Ozes, O. N., H. Akca, L. D. Mayo, J. A. Gustin, T. Maehama, J. E. Dixon, and D. B. Donner.** 2001. A phosphatidylinositol 3-kinase/Akt/mTOR pathway mediates and PTEN antagonizes tumor necrosis factor inhibition of insulin signaling through insulin receptor substrate-1. Proc. Natl. Acad. Sci. USA **98**:4640–4645.
43. **Rui, L., T. L. Fisher, J. Thomas, and M. F. White.** 2001. Regulation of insulin/insulin-like growth factor-1 signaling by proteasome-mediated degradation of insulin receptor substrate-2. J. Biol. Chem. **276**:40362–40367.
44. **Shimoike, T., S. Mimori, H. Tani, Y. Matsuura, and T. Miyamura.** 1999. Interaction of hepatitis C virus core protein with viral sense RNA and suppression of its translation. J. Virol. **73**:9718–9725.
45. **Shimomura, I., R. E. Hammer, J. A. Richardson, S. Ikemoto, Y. Bashmakov, J. L. Goldstein, and M. S. Brown.** 1998. Insulin resistance and diabetes mellitus in transgenic mice expressing nuclear SREBP-1c in adipose tissue: model for congenital generalized lipodystrophy. Genes Dev. **12**:3182–3194.
46. **Shimomura, I., M. Matsuda, R. E. Hammer, Y. Bashmakov, M. S. Brown, and J. L. Goldstein.** 2000. Decreased IRS-2 and increased SREBP-1c lead to mixed insulin resistance and sensitivity in livers of lipodystrophic and ob/ob mice. Mol. Cell **6**:77–86.
47. **Shintani, Y., H. Fujie, H. Miyoshi, T. Tsutsumi, K. Tsukamoto, S. Kimura, K. Moriya, and K. Koike.** 2004. Hepatitis C virus infection and diabetes: direct involvement of the virus in the development of insulin resistance. Gastroenterology **126**:840–848.
48. **Shulman, G. I.** 2000. Cellular mechanisms of insulin resistance. J. Clin. Investig. **106**:171–176.
49. **Su, A. I., J. P. Pezacki, L. Wodicka, A. D. Brideau, L. Supekova, R. Thimme, S. Wieland, J. Bukh, R. H. Purcell, P. G. Schultz, and F. V. Chisari.** 2002. Genomic analysis of the host response to hepatitis C virus infection. Proc. Natl. Acad. Sci. USA **99**:15669–15674.
50. **Sun, X. J., J. L. Goldberg, L. Y. Qiao, and J. J. Mitchell.** 1999. Insulin-induced insulin receptor substrate-1 degradation is mediated by the proteasome degradation pathway. Diabetes **48**:1359–1364.
51. **Suzuki, R., S. Sakamoto, T. Tsutsumi, A. Rikimaru, K. Tanaka, T. Shimoike, K. Moriishi, T. Iwasaki, K. Mizumoto, Y. Matsuura, T. Miyamura, and T. Suzuki.** 2005. Molecular determinants for subcellular localization of hepatitis C virus core protein. J. Virol. **79**:1271–1281.
52. **Tamemoto, H., T. Kadowaki, K. Tobe, T. Yagi, H. Sakura, T. Hayakawa, Y. Terauchi, K. Ueki, Y. Kaburagi, S. Satoh, et al.** 1994. Insulin resistance and growth retardation in mice lacking insulin receptor substrate-1. Nature **372**:182–186.
53. **Taniguchi, C. M., K. Ueki, and R. Kahn.** 2005. Complementary roles of IRS-1 and IRS-2 in the hepatic regulation of metabolism. J. Clin. Investig. **115**:718–727.
54. **Uysal, K. T., S. M. Wiesbrock, M. W. Marino, and G. S. Hotamisligil.** 1997. Protection from obesity-induced insulin resistance in mice lacking TNF-alpha function. Nature **389**:610–614.
55. **Vanhaesebroeck, B., and D. R. Alessi.** 2000. The PI3K-PDK1 connection: more than just a road to PKB. Biochem. J. **346**:561–576.

56. **White, M. F.** 1998. The IRS-signalling system: a network of docking proteins that mediate insulin action. Mol. Cell. Biochem. **182**:3–11.
57. **Withers, D. J., J. S. Gutierrez, H. Towery, D. J. Burks, J. M. Ren, S. Previs, Y. Zhang, D. Bernal, S. Pons, G. I. Shulman, S. Bonner-Weir, and M. F. White.** 1998. Disruption of IRS-2 causes type 2 diabetes in mice. Nature **391**:900–904.
58. **Yu, C., Y. Chen, G. W. Cline, D. Zhang, H. Zong, Y. Wang, R. Bergeron, J. K. Kim, S. W. Cushman, G. J. Cooney, B. Atcheson, M. F. White, E. W. Kraegen, and G. I. Shulman.** 2002. Mechanism by which fatty acids inhibit insulin activation of insulin receptor substrate-1 (IRS-1)-associated phosphatidylinositol 3-kinase activity in muscle. J. Biol. Chem. **277**: 50230–50236.

doi:10.1038/nature04734

nature

LETTERS

Differential roles of MDA5 and RIG-I helicases in the recognition of RNA viruses

Hiroki Kato[1,3]*, Osamu Takeuchi[1,3]*, Shintaro Sato[3], Mitsutoshi Yoneyama[4], Masahiro Yamamoto[1], Kosuke Matsui[1], Satoshi Uematsu[1], Andreas Jung[1], Taro Kawai[3], Ken J. Ishii[3], Osamu Yamaguchi[5], Kinya Otsu[5], Tohru Tsujimura[6], Chang-Sung Koh[7], Caetano Reis e Sousa[8], Yoshiharu Matsuura[2], Takashi Fujita[4] & Shizuo Akira[1,3]

The innate immune system senses viral infection by recognizing a variety of viral components (including double-stranded (ds)RNA) and triggers antiviral responses[1,2]. The cytoplasmic helicase proteins RIG-I (retinoic-acid-inducible protein I, also known as Ddx58) and MDA5 (melanoma-differentiation-associated gene 5, also known as Ifih1 or Helicard) have been implicated in viral dsRNA recognition[3–7]. *In vitro* studies suggest that both RIG-I and MDA5 detect RNA viruses and polyinosine-polycytidylic acid (poly(I:C)), a synthetic dsRNA analogue[3]. Although a critical role for RIG-I in the recognition of several RNA viruses has been clarified[8], the functional role of MDA5 and the relationship between these dsRNA detectors *in vivo* are yet to be determined. Here we use mice deficient in MDA5 (*MDA5*$^{-/-}$) to show that MDA5 and RIG-I recognize different types of dsRNAs: MDA5 recognizes poly(I:C), and RIG-I detects *in vitro* transcribed dsRNAs. RNA viruses are also differentially recognized by RIG-I and MDA5. We find that RIG-I is essential for the production of interferons in response to RNA viruses including paramyxoviruses, influenza virus and Japanese encephalitis virus, whereas MDA5 is critical for picornavirus detection. Furthermore, *RIG-I*$^{-/-}$ and *MDA5*$^{-/-}$ mice are highly susceptible to infection with these respective RNA viruses compared to control mice. Together, our data show that RIG-I and MDA5 distinguish different RNA viruses and are critical for host antiviral responses.

Host pattern recognition receptors, such as Toll-like receptors (TLRs) and helicase family members, have an essential role in the recognition of molecular patterns specific for different viruses, including DNA, single-stranded (ss)RNA, dsRNA and glycoproteins[1,9,10]. dsRNA can be generated during viral infection as a replication intermediate for RNA viruses. TLR3, which localizes in the endosomal membrane, has been shown to recognize viral dsRNA as well as the synthetic dsRNA analogue poly(I:C) (refs 11, 12). The cytoplasmic proteins RIG-I and MDA5 have also been identified as dsRNA detectors[3–5,7,13]. RIG-I and MDA5 contain two caspase-recruitment domains (CARDs) and a DExD/H-box helicase domain. RIG-I recruits a CARD-containing adaptor, IPS-1 (also known as MAVS, VISA or Cardif)[14–17]. IPS-1 relays the signal to the kinases TBK1 and IKK-i, which phosphorylate interferon-regulatory factor-3 (IRF-3) and IRF-7, transcription factors essential for the expression of type-I interferons[18–22]. In contrast, TLR3 activates TBK1 and IKK-i through the TIR-domain-containing adaptor TRIF (also known as Ticam1)[12].

In vitro studies have shown that both RIG-I and MDA5 can bind to poly(I:C) and respond to poly(I:C) and RNA viruses[6]. We have generated *RIG-I*$^{-/-}$ mice, and show that RIG-I is essential eliciting the immune responses against several RNA viruses, including Newcastle disease virus (NDV), Sendai virus (SeV) and vesicular stomatitis virus (VSV), in various cells except for plasmacytoid dendritic cells (pDCs)[8]. Hepatitis C virus and Japanese encephalitis virus are also reported to be recognized by RIG-I *in vitro*[23,24].

The *in vivo* functional relationship between RIG-I and MDA5 remains to be determined. To investigate a functional role for MDA5 *in vivo*, we generated *MDA5*$^{-/-}$ mice and investigated viral recognition (Supplementary Fig. 1). In contrast to *RIG-I*$^{-/-}$ mice, which are mostly embryonic lethal, *MDA5*$^{-/-}$ mice are born in a mendelian ratio, grow healthily and do not show gross developmental abnormalities until 24 weeks of age. Flow cytometric analysis of leukocytes from the spleen and lymph nodes (staining for CD3, B220 and CD11c) revealed that the composition of lymphocytes and dendritic cells is similar in wild-type and *MDA5*$^{-/-}$ mice (data not shown).

TLR3, RIG-I and MDA5 have been implicated in the recognition of poly(I:C) and the subsequent induction of antiviral responses. However, their exact contribution to *in vivo* responses against dsRNA has yet to be clarified. We therefore examined the *in vivo* responses to poly(I:C) in mice lacking RIG-I, MDA5 or TRIF, or both MDA5 and TRIF. Administration of poly(I:C) led to rapid induction of the cytokines interferon-α (IFN-α), IFN-β, interleukin-6 (IL-6) and IL-12 in sera of both wild-type and *RIG-I*$^{-/-}$ mice (Fig. 1a and Supplementary Fig. 2a). In contrast, *MDA5*$^{-/-}$ mice failed to produce IFN-α and IFN-β in response to poly(I:C), and production of IL-6 and IL-12p40 was also significantly impaired (Fig. 1b). Although *Trif*$^{-/-}$ mice produced normal amounts of IFN-α, they also showed severely impaired production of IL-12p40 and partial impairment in IL-6 production. *MDA5*$^{-/-}$; *Trif*$^{-/-}$ double-knockout mice failed to induce IFN-α, IL-6 and IL-12p40 in response to poly(I:C). These results indicate that MDA5 is essential for poly(I:C)-induced IFN-α production and TLR3 signalling is critical for IL-12 production, whereas both MDA5 and TLR3 regulate IL-6 production.

[1]Department of Host Defense, [2]Department of Molecular Virology, Research Institute for Microbial Diseases, Osaka University, and [3]ERATO, Japan Science and Technology Agency, 3-1 Yamada-oka, Suita, Osaka 565-0871, Japan. [4]Department of Genetics and Molecular Biology, Institute for Virus Research, Kyoto University, 53 Kawahara-cho, Shogoin, Sakyo-ku, Kyoto 606-8507, Japan. [5]Department of Cardiovascular Medicine, Osaka University Graduate School of Medicine, 2-2 Yamada-oka, Suita, Osaka 565-0871, Japan. [6]Department of Pathology, Hyogo College of Medicine, 1-1 Mukogawa-cho, Nishinomiya, Hyogo 663-8501, Japan. [7]Department of Medical Technology, Shinshu University School of Allied Medical Sciences, 3-1-1 Asahi, Matsumoto 390-8621, Japan. [8]Immunobiology Laboratory, Cancer Research UK London Research Institute, Lincoln's Inn Fields Laboratories, 44 Lincoln's Inn Fields, London WC2A 3PX, UK.
*These authors contributed equally to this work.

When bone-marrow-derived dendritic cells generated by granulocyte–macrophage colony-stimulating factor (GMCSF) were incubated in the presence of poly(I:C), production of IFN-α and IFN-β was severely impaired in *MDA5*$^{-/-}$, but not in *RIG-I*$^{-/-}$ or *Trif*$^{-/-}$, GMCSF-DCs (Fig. 1c and Supplementary Fig. 2b). Even when poly(I:C) was transfected into GMCSF-DCs using lipofectamine, poly(I:C) induced IFN-β production in an MDA5-dependent, but not a RIG-I- or TRIF-dependent, manner (Fig. 1d). IFN-β production in response to poly(I:C) was also impaired in *MDA5*$^{-/-}$ mouse embryonic fibroblasts (MEFs) (Fig. 1e), indicating that poly(I:C) is primarily recognized by MDA5, not RIG-I and TLR3, in these cells.

dsRNAs transcribed *in vitro* (Supplementary Fig. 2c) also stimulated MEFs to produce IFN-β. Unlike for poly(I:C), wild-type and *MDA5*$^{-/-}$ MEFs produced comparable amounts of IFN-β (Fig. 1e) in response to *in vitro* transcribed dsRNAs. In contrast, *RIG-I*$^{-/-}$ MEFs did not produce detectable amounts of IFN-β, indicating that RIG-I is essential for the detection of *in vitro* transcribed dsRNAs. As RIG-I, but not MDA5, is responsible for IFN-β production in response to dsRNAs of various lengths, these helicases probably distinguish nucleotide structure or sequence, but not length. Together, these results indicate that MDA5 and RIG-I are involved in the detection of poly(I:C) and *in vitro* transcribed dsRNAs, respectively.

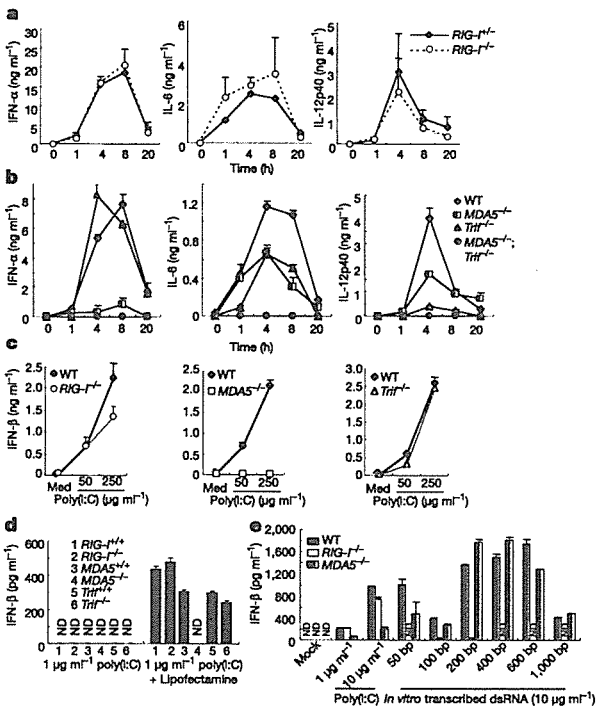

Figure 1 | Roles of MDA5, RIG-I and TRIF in the recognition of synthesized dsRNAs and dsRNA analogues. a, b, *RIG-I*$^{-/-}$ and littermate *RIG-I*$^{+/-}$ mice (**a**) or wild-type (WT), *MDA5*$^{-/-}$, *Trif*$^{-/-}$ or *MDA5*$^{-/-}$; *Trif*$^{-/-}$ double-knockout mice (**b**) were injected intravenously with 200 μg poly(I:C) for the indicated periods, and IFN-α, IL-6 and IL-12p40 production was measured in serum by ELISA. Data show mean ± s.d. **c**, GMCSF-DCs from *RIG-I*$^{-/-}$, *MDA5*$^{-/-}$, *TRIF*$^{-/-}$ and littermate control mice were incubated in the presence of 50 or 250 μg ml^{-1} poly(I:C) for 24 h. IFN-β production in the cell culture supernatants was measured by ELISA. Med, medium only. **d**, GMCSF-DCs were treated with 1 μg ml^{-1} poly(I:C) complexed with or without lipofectamine 2000 for 24 h, and IFN-β production was measured. **e**, Wild-type, *RIG-I*$^{-/-}$ and *MDA5*$^{-/-}$ MEFs were treated with poly(I:C) or *in vitro* transcribed dsRNAs of indicated lengths complexed with lipofectamine 2000 for 12 h, and IFN-β production was measured. Error bars indicate s.d. of triplicate wells in a single experiment; data are representative of three independent experiments. ND, not detected.

This finding led us to hypothesize that RIG-I and MDA5 are involved in the detection of different RNA viruses. We have previously shown that a set of negative-sense RNA viruses are recognized by RIG-I[8]. We first examined IFN-β and IFN-α production in *MDA5*$^{-/-}$ MEFs in response to a set of negative-sense ssRNA viruses, including NDV, SeV, VSV and influenza virus. As infection with most of the wild-type viruses (except NDV) failed to induce type-I interferons in MEFs, owing to suppression of interferon responses by viral proteins (data not shown), we also used mutant viruses lacking viral interferon-inhibitory proteins. As shown in Fig. 2a and Supplementary Fig. 4b, wild-type MEFs produce IFN-β and IFN-α in response to these mutant viruses. Production of type-I interferons was severely impaired in *RIG-I*$^{-/-}$ MEFs compared to wild-type cells, but MDA5 was dispensable for the production of type-I interferons. Japanese encephalitis virus (JEV), a positive-sense ssRNA virus belonging to the flavivirus family, also required RIG-I, but not MDA5, for IFN-β production (Fig. 2b).

We then examined the interferon responses of MEFs to encephalomyocarditis virus (EMCV), a positive-sense ssRNA virus belonging to the picornavirus family. EMCV-induced IFN-β production was abrogated in *MDA5*$^{-/-}$ MEFs (Fig. 2c). In contrast, wild-type and *RIG-I*$^{-/-}$ MEFs produced comparable amounts of IFN-β, indicating that EMCV is specifically recognized by MDA5. The induction of genes encoding IFN-β, IP-10 and IL-6 in response to EMCV was abrogated in *MDA5*$^{-/-}$ macrophages (Supplementary Fig. 3d). The synthesis of cellular proteins in *MDA5*$^{-/-}$ MEFs was progressively inhibited during EMCV infection, to an extent and with kinetics similar to wild-type MEFs (Supplementary Fig. 5), indicating that the EMCV infection was established in wild-type and *MDA5*$^{-/-}$ MEFs in a similar manner. Moreover, other viruses belonging to the picornavirus family (Theiler's and Mengo viruses) also induced IFN-α through MDA5 (Supplementary Fig. 4d). Furthermore, the production of IFN-β in response to SeV and EMCV was impaired in *RIG-I*$^{-/-}$ and *MDA5*$^{-/-}$ GMCSF-DCs, respectively (Fig. 2d, e), indicating that conventional dendritic cells (cDCs) also use these helicases for the differential recognition of viruses. EMCV-induced production of IL-6 was also abrogated in *MDA5*$^{-/-}$, but not *RIG-I*$^{-/-}$, cDCs (Supplementary Fig. 4c). Therefore, MDA5 is critical for the regulation of pro-inflammatory cytokines as well as type-I interferons in response to EMCV.

We next examined whether viral RNAs derived from VSV and EMCV recapitulate the production of interferons through MDA5 and RIG-I. When transfected into GMCSF-DCs by lipofection, RNAs prepared from VSV or EMCV induced production of IFN-α in a RIG-I- or MDA5-dependent manner, respectively (Fig. 2f). We also performed reconstitution experiments by transfecting RIG-I or MDA5 expression vectors into *RIG-I*$^{-/-}$; *MDA5*$^{-/-}$ MEFs, in which IFN-β induction was completely abrogated in response to infection with EMCV or SeV Cm (SeV with a mutated C protein) (Fig. 2g). The ectopic expression of human RIG-I, but not MDA5, activated the *Ifnb* promoter in response to SeV Cm. Reciprocally, cells expressing human MDA5, but not RIG-I, activated the *Ifnb* promoter in response to EMCV in a dose-dependent manner (Fig. 2h). These results indicate that human RIG-I and MDA5 recognize different RNA viruses by recognizing viral RNAs.

Previous studies have shown that pDCs use mainly the TLR system instead of RIG-I in the recognition of several RNA viruses[8]. MyD88 is an adaptor protein essential for TLR signalling (except through TLR3). We purified B220^{+} pDCs from Flt3L-generated bone-marrow-derived dendritic cells (Flt3L-DCs) and infected them with EMCV. pDCs from *Myd88*$^{-/-}$, but not *MDA5*$^{-/-}$, mice showed a profound defect in IFN-α production (Supplementary Fig. 6). Reciprocally, MDA5, but not MyD88, is required for the production of IFN-α in B220^{-} cDCs purified from Flt3L-DCs (Supplementary Fig. 6). These results indicate that both MDA5 and RIG-I are

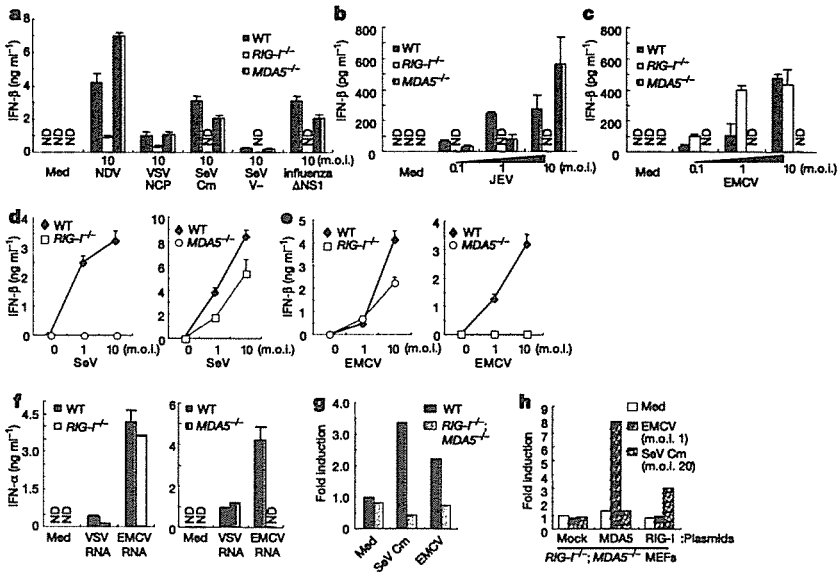

Figure 2 | Differential viral recognition by RIG-I and MDA5. **a**, Wild-type, *RIG-I*$^{-/-}$ and *MDA5*$^{-/-}$ MEFs were exposed to negative-sense ssRNA viruses, including NDV, VSV lacking a variant of M protein (NCP), SeV with a mutated C protein (Cm), SeV lacking V protein (V^{-}), and influenza virus lacking the NS1 protein (ΔNS1) for 24 h. IFN-β production in the culture supernatants was measured by ELISA. **b**, **c**, Wild-type, *RIG-I*$^{-/-}$ and *MDA5*$^{-/-}$ MEFs were exposed to the positive-sense ssRNA viruses JEV (**b**) and EMCV (**c**), and IFN-β production was measured. **d**, **e**, GMCSF-DCs from *RIG-I*$^{-/-}$ and *MDA5*$^{-/-}$ mice and their littermate wild-type mice were infected with an increasing m.o.i. of SeV V^{-} (**d**) or EMCV (**e**) for 24 h, and IFN-β production was measured. **f**, Wild-type, *RIG-I*$^{-/-}$ and *MDA5*$^{-/-}$ GMCSF-DCs were treated with RNAs directly prepared from VSV and EMCV (complexed with lipofectamine 2000) for 24 h, and IFN-α production was measured. **g**, Wild-type and *RIG-I*$^{-/-}$; *MDA5*$^{-/-}$ MEFs were transiently transfected with a reporter construct containing the *Ifnb* promoter and exposed to SeV Cm or EMCV for 24 h. Cell lysates were then prepared and subjected to a luciferase assay. **h**, RIG-I$^{-/-}$; MDA5$^{-/-}$ MEFs were transiently transfected with the *Ifnb* promoter construct together with expression plasmids encoding human RIG-I or MDA5. The cells were then infected with EMCV or SeV Cm for 24 h and were subjected to a luciferase assay. Error bars in **a**–**g** indicate s.d. of triplicate wells in a single experiment; data are representative of three independent experiments. ND, not detected.

dispensable for the viral induction of IFN-α in pDCs.

We next examined the *in vivo* roles of MDA5 and RIG-I in host defence against viral infection. Although most *RIG-I*$^{-/-}$ mice are embryonic lethal[8], we could efficiently obtain live adult mice by intercrossing the *RIG-I*$^{+/-}$ mice obtained after *RIG-I*$^{+/-}$ × ICR crosses (Supplementary Table 1). When the mice were infected with JEV, serum IFN-α levels were markedly decreased in *RIG-I*$^{-/-}$ mice compared to littermate *RIG-I*$^{+/-}$ mice. In contrast, *MDA5*$^{-/-}$ mice did not show a defect in JEV-induced systemic IFN-α production (Fig. 3a). IFN-α production was partially impaired in *Myd88*$^{-/-}$ mice compared to wild-type mice, but the extent of this impairment was far less than in *RIG-I*$^{-/-}$ mice (Fig. 3a). These data suggest that the TLR system is not critical for the induction of serum IFN-α *in vivo* in response to JEV. Consistent with this finding, *RIG-I*$^{-/-}$ mice, but not *MDA5*$^{-/-}$ or *Myd88*$^{-/-}$ mice, were more susceptible to JEV infection than control mice (Fig. 3b). Furthermore, *RIG-I*$^{-/-}$ mice, but not *MDA5*$^{-/-}$ mice, succumbed to VSV infection, consistent with abrogated interferon responses (Supplementary Fig. 7). Thus, RIG-I-mediated recognition of a specific set of viruses has a critical role in antiviral host defence *in vivo*.

We next challenged the mice with EMCV as a model virus that is recognized by MDA5. Induction of IFN-β, IFN-α, RANTES and IL-6 was severely impaired in the sera of *MDA5*$^{-/-}$ mice (Fig. 4a and Supplementary Fig. 8). *MDA5*$^{-/-}$ mice and mice null for the IFN-α/β receptor (*Ifnar1*$^{-/-}$) were highly susceptible to EMCV infection (viral titre of 1×10^2 plaque-forming units (p.f.u.)) compared to littermate controls ($P < 0.01$) (Fig. 4b). In contrast, deficiency of neither RIG-I nor TLR3 affected the survival of mice infected with EMCV. Consistent with a previous report[22], *Myd88*$^{-/-}$ mice were modestly susceptible to EMCV infection compared to wild-type mice, implying that pDC-mediated responses are not critical for eliminating EMCV (Fig. 4b).

It is known that EMCV preferentially infects cardiomyocytes and causes myocarditis. Consistent with increased susceptibility to EMCV, viral titre in the heart was much higher in *MDA5*$^{-/-}$ mice compared to control mice (Fig. 4c). Histological analysis of hearts two days after EMCV infection revealed that focal necrosis of

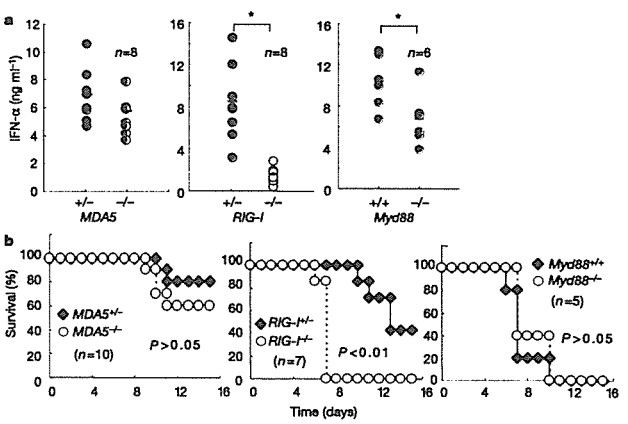

Figure 3 | Susceptibility of *RIG-I*$^{-/-}$ and *MDA5*$^{-/-}$ mice to JEV infection. **a**, *RIG-I*$^{+/-}$, *RIG-I*$^{-/-}$, *MDA5*$^{+/-}$ and *MDA5*$^{-/-}$ mice ($n = 8$), and *Myd88*$^{+/+}$ or *Myd88*$^{-/-}$ mice ($n = 6$), were injected intravenously with 2×10^7 p.f.u. JEV. Sera were collected 24 h after injection, and IFN-α production levels measured by ELISA. Circles represent individual mice, bars indicate mean values. Asterisk, $P < 0.05$ versus controls (*t*-test). **b**, The survival of 6-week-old mice (genotypes as indicated) infected intravenously with 2×10^7 p.f.u. JEV. Mice were monitored for 15 days ($P < 0.01$ between *RIG-I*$^{-/-}$ mice and their littermate controls, generalized Wilcoxon test).

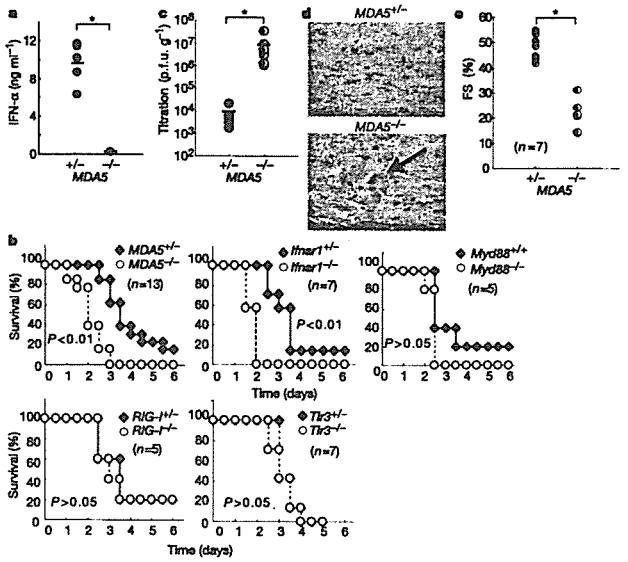

Figure 4 | Role of MDA5 in host defence against EMCV infection. **a**, $MDA5^{+/-}$ and $MDA5^{-/-}$ mice ($n = 5$) were inoculated intravenously with 1×10^7 p.f.u. EMCV. Sera were prepared 4 h after injection and IFN-α production levels determined by ELISA. **b**, The survival of 6-week-old mice (genotypes as indicated) infected with 1×10^2 p.f.u. EMCV intraperitoneally was monitored every 12 h for six days ($P < 0.01$ between $MDA5^{-/-}$ or $Ifnar1^{-/-}$ mice and their littermate controls, generalized Wilcoxon test). **c**, $MDA5^{+/-}$ and $MDA5^{-/-}$ mice were infected intraperitoneally with 1×10^2 p.f.u. EMCV. After 48 h, mice were killed and virus titres in hearts were determined by plaque assay. **d**, Heart sections of $MDA5^{+/-}$ and $MDA5^{-/-}$ mice, two days after infection, were assessed for histological changes using haematoxylin and eosin staining. Arrow indicates the focal necrosis of cardiomyocytes. **e**, Cardiac function of mice 48 h after EMCV infection was assessed by echocardiography (see Supplementary Fig. 8b). The fractional shortening (FS) after infection determined by transthoracic M-mode echocardiographic tracings is shown. Asterisk, $P < 0.05$ versus $MDA5^{+/-}$ mice (*t*-test).

cardiomyocytes had developed in $MDA5^{-/-}$ mice, but wild-type hearts showed no histological abnormalities at this time point (Fig. 4d). Notably, no infiltration of immune cells was observed in either wild-type or $MDA5^{-/-}$ heart sections at this time point. However, when cardiac performance was analysed by echocardiography two days after infection (Fig. 4e), cardiac contractility was severely depressed in $MDA5^{-/-}$ mice (fractional shortening 48.2 ± 4.9% in $MDA5^{+/-}$ mice, 21.2 ± 5.8% in $MDA5^{-/-}$ mice), indicating that $MDA5^{-/-}$ mice developed severe heart failure due to virus-induced cardiomyopathy. Thus, MDA5-mediated recognition of EMCV is a prerequisite for triggering antiviral responses as well as for prevention of myocardial dysfunction.

Together, our results demonstrate that RIG-I and MDA5 have essential roles in the recognition of different groups of RNA viruses, as well as in the subsequent production of type-I interferons and pro-inflammatory cytokines. We have found that poly(I:C) and *in vitro* transcribed dsRNA are recognized by MDA5 and RIG-I, respectively; this is in contrast to results from previous *in vitro* studies. RIG-I probably recognizes dsRNA generated over the course of RNA virus replication, as all *in vitro* transcribed dsRNAs tested except for poly(I:C) induced type-I interferons through RIG-I. In contrast, the endogenous ligand of MDA5 remains enigmatic. Moreover, how RIG-I and MDA5 differentially recognize natural dsRNAs is undetermined. Given that the helicase domains of RIG-I and MDA5 bind to dsRNA, analyses of the crystal structures of these domains should to help achieve a better understanding of the molecular mechanisms underlying this differential recognition. Furthermore, it is still possible that unknown dsRNA-binding proteins also function as direct receptors for viral RNAs.

Finally, the picornavirus family contains several viruses that are pathogenic for humans, including poliovirus, rhinovirus and the virus causing foot-and-mouth-disease. Our studies suggest that human MDA5 and RIG-I also recognize RNA viruses. Thus, identification of therapeutic agents that modify RIG-I or MDA5 may lead to antiviral strategies against selected viruses.

METHODS

Mice, cells and reagents. The generation of $MDA5^{-/-}$ mice is described in the Supplementary Information. $Myd88^{-/-}$, $Tlr3^{-/-}$ and $Trif^{-/-}$ mice have been described previously[12]. $Ifnar1^{-/-}$ mice have also been described previously[25]. $RIG\text{-}I^{+/-}$ mice in a 129Sv × C57BL/6 background were crossed with ICR mice, and the resulting $RIG\text{-}I^{+/-}$ mice were further intercrossed. Interbreeding of these $RIG\text{-}I^{+/-}$ mice produced healthy and fertile $RIG\text{-}I^{-/-}$ offspring, although their number was less than half that of $RIG\text{-}I^{+/+}$ progeny (Supplementary Table 1). $RIG\text{-}I^{-/-}$ and $RIG\text{-}I^{+/-}$ littermate mice were used for *in vivo* experiments. $RIG\text{-}I^{-/-}$; $MDA5^{-/-}$ mice in a 129Sv × C57BL/6 background were lethal at embryonic day 12.5. Additional details regarding cells, reagents and the preparation of *in vitro* transcribed dsRNA are provided in the Supplementary Information.

Viruses. NDV (ref. 3), VSV, VSV lacking a variant of M protein (NCP) (ref. 8), influenza virus lacking the NS1 protein (ΔNS1) (ref. 26), JEV (ref. 27) and EMCV (ref. 3) have been described previously. SeV and SeV lacking the V protein (V^-) or with mutated C proteins (Cm) were provided by A. Kato[28].

Luciferase assay. Wild-type or $RIG\text{-}I^{-/-}$; $MDA5^{-/-}$ MEFs were transiently transfected with a reporter construct containing the *Ifnb* promoter together with an empty vector (mock), or *RIG-I* or *MDA5* expression vectors. As an internal control, a *Renilla* luciferase construct was transfected. Transfected cells were untreated or infected with EMCV or SeV Cm (m.o.i. 20) for 24 h. The cells were lysed and subjected to a luciferase assay using a dual-luciferase reporter assay system (Promega) according to the manufacturer's instructions.

Analysis of mice after EMCV infection. Methods for plaque assays, histological analysis and echocardiography are described in the Supplementary Information.

Measurement of cytokine production. Cell culture supernatants were collected and analysed for IFN-β, IFN-α, IL-6 or IL-12p40 production using enzyme-linked immunosorbent assays (ELISAs). ELISA kits for mouse IFN-α and IFN-β were purchased from PBL Biomedical Laboratories, and those for IL-6, IL-12p40 and RANTES were obtained from R&D Systems.

Statistical analysis. Kaplan–Meier plots were constructed and a generalized Wilcoxon test was used to test for differences in survival between control and mutant mice after viral infection. Statistical significance of any differences in cytokine concentration and ECMV titres was determined using Student's *t*-tests.

Received 30 January; accepted 20 March 2006.
Published online 9 April 2006.

1. Akira, S., Uematsu, S. & Takeuchi, O. Pathogen recognition and innate immunity. *Cell* 124, 783–801 (2006).
2. Katze, M. G., He, Y. & Gale, M. Jr. Viruses and interferon: A fight for supremacy. *Nature Rev. Immunol.* 2, 675–687 (2002).
3. Yoneyama, M. *et al.* The RNA helicase RIG-I has an essential function in double-stranded RNA-induced innate antiviral responses. *Nature Immunol.* 5, 730–737 (2004).
4. Kang, D. C. *et al. mda-5*: An interferon-inducible putative RNA helicase with double-stranded RNA-dependent ATPase activity and melanoma growth-suppressive properties. *Proc. Natl Acad. Sci. USA* 99, 637–642 (2002).
5. Andrejeva, J. *et al.* The V proteins of paramyxoviruses bind the IFN-inducible RNA helicase, mda-5, and inhibit its activation of the *IFN-β* promoter. *Proc. Natl Acad. Sci. USA* 101, 17264–17269 (2004).
6. Yoneyama, M. *et al.* Shared and unique functions of the DExD/H-box helicases RIG-I, MDA5, and LGP2 in antiviral innate immunity. *J. Immunol.* 175, 2851–2858 (2005).
7. Rothenfusser, S. *et al.* The RNA helicase Lgp2 inhibits TLR-independent sensing of viral replication by retinoic acid-inducible gene-I. *J. Immunol.* 175, 5260–5268 (2005).
8. Kato, H. *et al.* Cell type-specific involvement of RIG-I in antiviral response. *Immunity* 23, 19–28 (2005).
9. Iwasaki, A. & Medzhitov, R. Toll-like receptor control of the adaptive immune responses. *Nature Immunol.* 5, 987–995 (2004).
10. Beutler, B. Inferences, questions and possibilities in Toll-like receptor signalling. *Nature* 430, 257–263 (2004).
11. Alexopoulou, L., Holt, A. C., Medzhitov, R. & Flavell, R. A. Recognition of double-stranded RNA and activation of NF-κB by Toll-like receptor 3. *Nature* 413, 732–738 (2001).

12. Yamamoto, M. *et al.* Role of adaptor TRIF in the MyD88-independent toll-like receptor signaling pathway. *Science* **301**, 640–643 (2003).
13. Kovacsovics, M. *et al.* Overexpression of Helicard, a CARD-containing helicase cleaved during apoptosis, accelerates DNA degradation. *Curr. Biol.* **12**, 838–843 (2002).
14. Kawai, T. *et al.* IPS-1, an adaptor triggering RIG-I- and Mda5-mediated type I interferon induction. *Nature Immunol.* **6**, 981–988 (2005).
15. Seth, R. B., Sun, L., Ea, C. K. & Chen, Z. J. Identification and characterization of MAVS, a mitochondrial antiviral signaling protein that activates NF-κB and IRF 3. *Cell* **122**, 669–682 (2005).
16. Xu, L. G. *et al.* VISA is an adapter protein required for virus-triggered IFN-β signaling. *Mol. Cell* **19**, 727–740 (2005).
17. Meylan, E. *et al.* Cardif is an adaptor protein in the RIG-I antiviral pathway and is targeted by hepatitis C virus. *Nature* **437**, 1167–1172 (2005).
18. Fitzgerald, K. A. *et al.* IKKε and TBK1 are essential components of the IRF3 signaling pathway. *Nature Immunol.* **4**, 491–496 (2003).
19. Sharma, S. *et al.* Triggering the interferon antiviral response through an IKK-related pathway. *Science* **300**, 1148–1151 (2003).
20. Hemmi, H. *et al.* The roles of two IκB kinase-related kinases in lipopolysaccharide and double stranded RNA signaling and viral infection. *J. Exp. Med.* **199**, 1641–1650 (2004).
21. Sato, M. *et al.* Distinct and essential roles of transcription factors IRF-3 and IRF-7 in response to viruses for IFN-α/β gene induction. *Immunity* **13**, 539–548 (2000).
22. Honda, K. *et al.* IRF-7 is the master regulator of type-I interferon-dependent immune responses. *Nature* **434**, 772–777 (2005).
23. Chang, T. H., Liao, C. L. & Lin, Y. L. Flavivirus induces interferon-beta gene expression through a pathway involving RIG-I-dependent IRF-3 and PI3K-dependent NF-κB activation. *Microbes Infect.* **8**, 157–171 (2006).
24. Melchjorsen, J. *et al.* Activation of innate defense against a paramyxovirus is mediated by RIG-I and TLR7 and TLR8 in a cell-type-specific manner. *J. Virol.* **79**, 12944–12951 (2005).
25. Hoshino, K., Kaisho, T., Iwabe, T., Takeuchi, O. & Akira, S. Differential involvement of IFN-β in Toll-like receptor-stimulated dendritic cell activation. *Int. Immunol.* **14**, 1225–1231 (2002).
26. Diebold, S. S., Kaisho, T., Hemmi, H., Akira, S. & Reis e Sousa, C. Innate antiviral responses by means of TLR7-mediated recognition of single-stranded RNA. *Science* **303**, 1529–1531 (2004).
27. Mori, Y. *et al.* Nuclear localization of Japanese encephalitis virus core protein enhances viral replication. *J. Virol.* **79**, 3448–3458 (2005).
28. Kato, A. *et al.* Characterization of the amino acid residues of sendai virus C protein that are critically involved in its interferon antagonism and RNA synthesis down-regulation. *J. Virol.* **78**, 7443–7454 (2004).

Supplementary Information is linked to the online version of the paper at www.nature.com/nature.

Acknowledgements We thank all colleagues in our laboratory, K. Takeda, T. Shioda, E. Nakayama and K. Kiyotani for helpful discussions, A. Kato, T. Abe, Y. Mori, B. S. Kim and A. Palmenberg for viruses and plasmids, M. Hashimoto for secretarial assistance, and Y. Fujiwara, M. Shiokawa, N. Kitagaki and A. Shibano for technical assistance. This work was supported by grants from the Ministry of Education, Culture, Sports, Science and Technology in Japan, and from the 21st Century Center of Excellence Program of Japan.

Author Information Reprints and permissions information is available at npg.nature.com/reprintsandpermissions. The authors declare no competing financial interests. Correspondence and requests for materials should be addressed to S.A. (sakira@biken.osaka-u.ac.jp).

Supplementary Information

I. Supplementary Materials and Methods

II. Supplemental Figure Legends

III. Supplemental Figures

I. Supplementary Materials and Methods

Generation of MDA5$^{-/-}$ mice

The MDA5 gene was isolated from genomic DNA extracted from ES cells (GSI-I) by PCR. The targeting vector was constructed by replacing a 4.3-kb fragment encoding the MDA5 ORF (including DExH box) with a neomycin-resistance gene cassette (*neo*), and a herpes simplex virus thymidine kinase (HSV-TK) driven by PGK promoter was inserted into the genomic fragment for negative selection. After the targeting vector was transfected into ES cells, G418 and gancyclovir doubly resistant colonies were selected and screened by PCR and further confirmed by Southern blotting. Homologous recombinants were micro-injected into C57BL/6 female mice, and heterozygous F1 progenies were intercrossed in order to obtain MDA5$^{-/-}$ mice. MDA5$^{-/-}$ and littermate control mice were used throughout the experiments.

Cells and Reagents

RIG-I$^{-/-}$ or MDA5$^{-/-}$ MEFs were prepared from embryos under 129Sv and C57BL/6 background derived at 12.5 days postcoitum. RIG-I$^{-/-}$MDA5$^{-/-}$ MEFs were prepared from embryos (129Sv X C57BL/6 background) at 11.5 days postcoitum. Bone marrow derived DCs were generated in RPMI 1640 medium containing 10% FCS, 50 mM 2-mercaptoethanol, and 10 ng/ml GM-CSF or 10 ng/ml Flt3L. pDCs and cDCs were isolated from Flt3L-DCs by MACS using anti-B220 and CD11c microbeads from

Miltenyi Biotech as described. Poly I:C was purchased from Amersham Biosciences. For the synthesis of poly I:C, poly I (152-539 bases) and poly C (319-1305 bases) have been separately synthesized and then annealed. Therefore, the expected length of poly I:C is 319-539 bps (Amersham Bisciences). Poly I:C was complexed with cationic lipids, Lipofectamin 2000 reagents (Invitrogen), and added to MEFs. DCs were incubated with or without Lipofectamine 2000 for stimulation.

Northern blot

PECs were treated with or without 1000 U/ml mouse IFN-β (Calbiochem) for 8 h, and total RNA was extracted using TRIzol reagent (Invitrogen). RNA was electrophoresed, transferred to nylon membranes and then hybridized with indicated cDNA probes. To detect the expression of MDA5 mRNA, a 308 bp fragment (777-1084) was used as a probe. The same membrane was rehybridized with a β-actin probe.

Western blot analysis and an antibody

MEF were treated with 1000 U/ml IFN-β for 8 h. Cells were then lysed in a lysis buffer containing 1.0% Nonidet-P40, 150 mM NaCl, 20 mM Tris-Cl (pH7.5), 1 mM EDTA and protease inhibitor cocktail (Roche). Cell lysates were dissolved by SDS-PAGE and transferred onto a PVDF membrane. The membrane was blotted with the specific antibody to MDA5 protein, and visualized with an enhanced chemiluminescence system (Perkinermer). Polyclonal anti-MDA5 antibody was raised against corresponding to amino acids 1005-1019 of mouse MDA5.

Preparation of in vitro transcribed dsRNA

The mouse Lamin A/C cDNA sequence was amplified by PCR and cloned into the pT7 blue T vector (Novagen) and sequenced. Various lengths of dsRNAs corresponding to the sequence of mouse Lamin A/C were generated using a T7 RiboMAX^{TM} Express RNAi

System (Promega) according to the manufacturer's instruction. In brief, DNA fragments tagged with T7 RNA polymerase promoters corresponding to parts of Lamin A/C (50, 100, 200, 400, 600, 1000 bps) were amplified by a PCR reaction using Lamin A/C cDNA as a template, and with following primers;

T7 Lamin. Forward, TAATACGACTCACTATAGGacttgttggctgcgcaggc

T7 Lamin.50 reverse, TAATACGACTCACTATAGGtgagaagagcctcgaggtcctt

T7 Lamin.100 reverse, TAATACGACTCACTATAGGcaatgtgcgcttctcactgagagcag

T7 Lamin.200 reverse, TAATACGACTCACTATAGGccactcgcctcagcatctcat

T7 Lamin.400 reverse, TAATACGACTCACTATAGGctgttccacctggtcctcatg

T7 Lamin.600 reverse, TAATACGACTCACTATAGGtcctccaggtcacgcagcttt

T7 Lamin.1000 reverse, TAATACGACTCACTATAGGggacttgttgcgcagccgcacgaac

The PCR products were purified and used as templates for in vitro transcription with T7 RNA polymerase. The product was annealed to form dsRNA followed by treatment with DNase and RNase to digest ssRNA and DNA. The dsRNA was further purified by isopropanol precipitation and resuspended in Nucrease-free water. The generation of dsRNAs was visualized by Agarose gel electrophoresis (Supplementary Fig. 2b). To stimulate MEFs, the dsRNA was complexed with Lipofectamine 2000, then added to the cells, and incubated for 24 hours.

Histological analysis

Hearts were taken from EMCV infected mice, and fixed with 3.7% formaldehyde. Transverse sections through the heart (5 μm) were cut and stained with hematoxylin and eosin.

Plaque assay

Forty-eight hours after EMCV infection, Hearts were prepared and homogenized in PBS. Virus titration in the virus containing PBS was determined by standard plaque assay as

described previously[8]. After centrifugation, supernatants were serially diluted, and added to plates containing HeLa cells. The cells were overlaid with DMEM containing 1% low melting agarose and incubated for 48 h. Then plaques were counted.

Echocardiography

Two days after EMCV infection, echocardiography was performed on mice anesthetized with 2.5% avertin (8 μl/g) using ultra-sonography (SONOS-5500, equipped with a 15-MHz linear transducer, Philips Medical Systems). Hearts were imaged in a two-dimensional parasternal short-axis view, and an M-mode echocardiogram of the midventricle was recorded at the level of the papillary muscles*. Heart rate, anterior and posterior wall thickness, and end-diastolic and end-systolic internal dimensions of the LV were obtained from the M-mode image.

Viruses

Mengo virus[1] was kindly provided by A. Palmenberg. Theiler's virus[2] have been described previously.

Preparation of viral RNA.

BHK cells and L cell plated on 10 X 15 cm dishes were infected with moi= 0.01 of wt VSV and EMCV, respectively. At 1h after infection, medium was removed and replaced with DMEM containing 10 % FCS and the cells were incubated for 2 days at 37 °C. Then the supernatants were collected and centrifuged at 3,000 rpm for 15 min to remove cells for avoiding cellar RNA contamination. Then the supernatants were harvested and centrifuged at 25,000 rpm for 90 min in an SW28 rotor at 4 °C. The viral pellet was suspended in TRIzol reagent (Invitrogen) and RNA was extracted. 5-10 μg/ml VSV RNA and 0.5-3 μg/ml EMCV RNA were obtained from single preparation.

Analysis of total protein synthesis.

Cultures of wild-type and MDA5$^{-/-}$ MEFs were infected with EMCV. At various time of labeled by incorporation of 50 μCi of [^{35}S]Met-Cys (GE Healthcare) for 1 h. Then the cells were lysed in a lysis buffer containing 1.0% Nonidet-P40, 150 mM NaCl, 20 mM Tris-Cl (pH7.5), 1 mM EDTA and protease inhibitor cocktail (Roche). Total cell extracts were separated by polyacrylamide gel electrophoresis, and the proteins were visualized by autoradiography.

1. Martin, L. R., Neal, Z. C., McBride, M. S. & Palmenberg, A. C. Mengovirus and encephalomyocarditis virus poly(C) tract lengths can affect virus growth in murine cell culture. J Virol 74, 3074-81 (2000).
2. Shin, T. & Koh, C. S. Immunohistochemical detection of osteopontin in the spinal cords of mice with Theiler's murine encephalomyelitis virus-induced demyelinating disease. Neurosci Lett 356, 72-4 (2004).

II. Supplemental Figure Legends

Supplementary Fig. 1: Targeted disruption of the murine MDA5 gene.

(a) Structure of the mouse *MDA5* gene, the targeting vector and the predicted disrupted gene. Closed boxes denote the coding exon. B; BamH I (b) Southern blot analysis of offspring from the heterozygote intercrosses. Genomic DNA was extracted from mouse tails, digested with BamHI, separated by electrophoresis and hybridized with the radiolabelled probe indicated in (a). Southern blot gave a single 9.4 kb band for wild-type (+/+), a 4.6 kb band for homozygous (-/-) and both bands for heterozygous (+/-) mice. (c) Nothern blot analysis of peritoneal exudates cells (PECs). Total RNA from wild-type (WT) and MDA5$^{-/-}$ PECs treated with 1000 U/ml IFN-β for 8 h was extracted and subjected to Northern blot analysis for the expression of *MDA5* mRNA. The same

membrane was rehybridized with a *β-actin* probe. (d) Western blot analysis of MDA5 expression. WT and MDA5$^{-/-}$ MEFs were treated with 1000 U/ml IFN-β for 8 h, and whole cell lysates were immunoblotted with antibody against MDA5. N.S. non specific.

Supplementary Fig. 2. Involvement of MDA5 or RIG-I in the recognition of dsRNAs.

(a) RIG-I$^{-/-}$ and MDA5$^{-/-}$, and their littermate WT mice were injected intravenously with 200 μg of poly I:C for the indicated periods and the production of IFN-β in the sera was measured by ELISA. The data are means ± S.D. of sera samples.

(b) GMCSF-DCs from RIG-I$^{-/-}$ and MDA5$^{-/-}$, TRIF$^{-/-}$ and their littermate control mice were incubated in the presence of 50, 250 μg/ml poly I:C for 24 h. The production of IFN-α in the culture supernatants was measured by ELISA.

(c) Generation of different lengths of dsRNAs corresponding to mouse lamin A/C. Different lengths of dsRNAs corresponding to mouse lamin A/C were synthesized as described in Methods section. 1 μg of dsRNAs were separated on 1% Agarose gel and visualized by staining with ethidium bromide. All dsRNAs synthesized appear with the estimated size.

Supplementary Fig. 3: Contribution of RIG-I and MDA5 in the induction of genes encoding type I IFNs and IFN-inducible proteins in response to viral infection.

(a) WT, RIG-I$^{-/-}$ or MDA5$^{-/-}$ MEFs were treated with 5 μg/ml poly I:C complexed with lipofectamine 2000 for the indicated periods. Total RNA was extracted and subjected to the Northern blot analysis for the expression of *IFN-β*, *IP10* and *β-actin* mRNA.

(b) WT, RIG-I$^{-/-}$ and MDA5$^{-/-}$ MEFs were treated with 5 μg/ml dsRNA corresponding to Lamin A/C (600 bps) complexed with lipofectamine 2000 for the indicated periods. Total RNA was extracted and subjected to the Northern blot analysis for the expression of

IFN-β and *IP10* mRNA. 28S and 18S ribosomal RNA bands on ethidium bromide-stained gel were used to control the RNA loading (lower panel).

(c) WT, RIG-I$^{-/-}$ and MDA5$^{-/-}$ MEFs were infected with moi=10 of SeV V(-) for the indicated periods. Total RNA was extracted and subjected to the Northern blot analysis for the expression of *IFN-β* and *IP10* mRNA. 28S and 18S ribosomal RNA bands on ethidium bromide-stained gel were used to control the RNA loading (lower panel).

(d) WT and MDA5$^{-/-}$ PECs were exposed to moi=10 of EMCV for the indicated periods. Total RNA was extracted and subjected to the Northern blot analysis for the expression of *IFN-β*, *IP10*, *IL-6* and *β-actin* mRNA.

Supplementary Fig. 4: Role of MDA5 and RIG-I in the IFN-α responses against various viruses.

(a) WT, RIG-I$^{-/-}$ and MDA5$^{-/-}$ MEFs were exposed to negative-sense ssRNA viruses, including NDV, VSV NCP, SeV Cm, SeV V- and influenza ΔNS1. IFN-α production in the culture supernatants was measured by ELISA.

(b and c) GMCSF-DCs from RIG-I$^{-/-}$ and MDA5$^{-/-}$ mice and their littermate WT mice were infected with indicated moi of EMCV for 24 h. The production of IFN-α (b) and IL-6 (c) in the culture supernatants was measured by ELISA.

(d) GMCSF-DCs from wild-type and MDA5$^{-/-}$ mice were infected with indicated moi of Theiler's virus or Mengovirus for 24 h. IFN-α production in the culture supernatants was measured by ELISA. The data are means ± S.D. of tripricates.

Supplementary Fig. 5: EMCV-mediated protein synthesis shutoff was not altered between wild-type and MDA5$^{-/-}$ MEFs.

Cultures of wild-type and MDA5$^{-/-}$ MEFs were infected with EMCV and labeled by incorporation of [^{35}S]Met-Cys for 1 h at various times after infection. Total cell extracts

were separated by polyacrylamide gel electrophoresis, and the proteins were visualized by autoradiography.

Supplementary Fig. 6: Differential involvement of MDA5 and MyD88 in EMCV-mediated IFN production in cDCs and pDCs.

DCs were induced from bone marrow cells obtained from $MyD88^{+/-}$, $MyD88^{-/-}$, $MDA5^{+/-}$ and $MDA5^{-/-}$ mice by cultivating in the presence of Flt3L. At day 7, $B220^{+}CD11c^{+}$ pDCs and $B220^{-}CD11c^{+}$ cDCs were purified by MACS, and infected with EMCV for 24h. IFN-α production in the culture supernatants was measured by ELISA. Error bars indicate ± S.D. of triplicates.

Supplementary Fig. 7: The survival of $MDA5^{-/-}$, $RIG\text{-}I^{-/-}$ or $IFN\alpha/\beta R^{-/-}$ mice in response to VSV infection.

The survival of the mice (3-weeks old) infected with $4x10^{6}$ pfu VSV intranasally was monitored for 9 days ($p<0.01$ by the generalized wilcoxon test between $RIG\text{-}I^{-/-}$ mice and their littermate controls).

Supplementary Fig. 8: Responses of $MDA5^{-/-}$ mice against EMCV infection

(a) $MDA5^{+/-}$ and $MDA5^{-/-}$ mice (n=5) were intravenously inoculated with 1 X 10^{7} pfu EMCV. Sera were taken at 4 h after injection, and IFN-β, Rantes and IL-6 production levels were determined by ELISA. *, $P<0.05$ versus controls by the student's t-test.

(b) Cardiac function of the mice 48 h after EMCV infection was assessed by echocardiography. Transthoracic M-mode echocardiographic tracings from $MDA5^{+/-}$ and $MDA5^{-/-}$ mice 48 h after EMCV infection.

Supplementary Table I: Genotypes of mice derived from $RIG\text{-}I^{+/-}$ intercrosses or crosses between $RIG\text{-}I^{+/-}$ and $RIG\text{-}I^{-/-}$ mice.

Supplemental Figure 1.

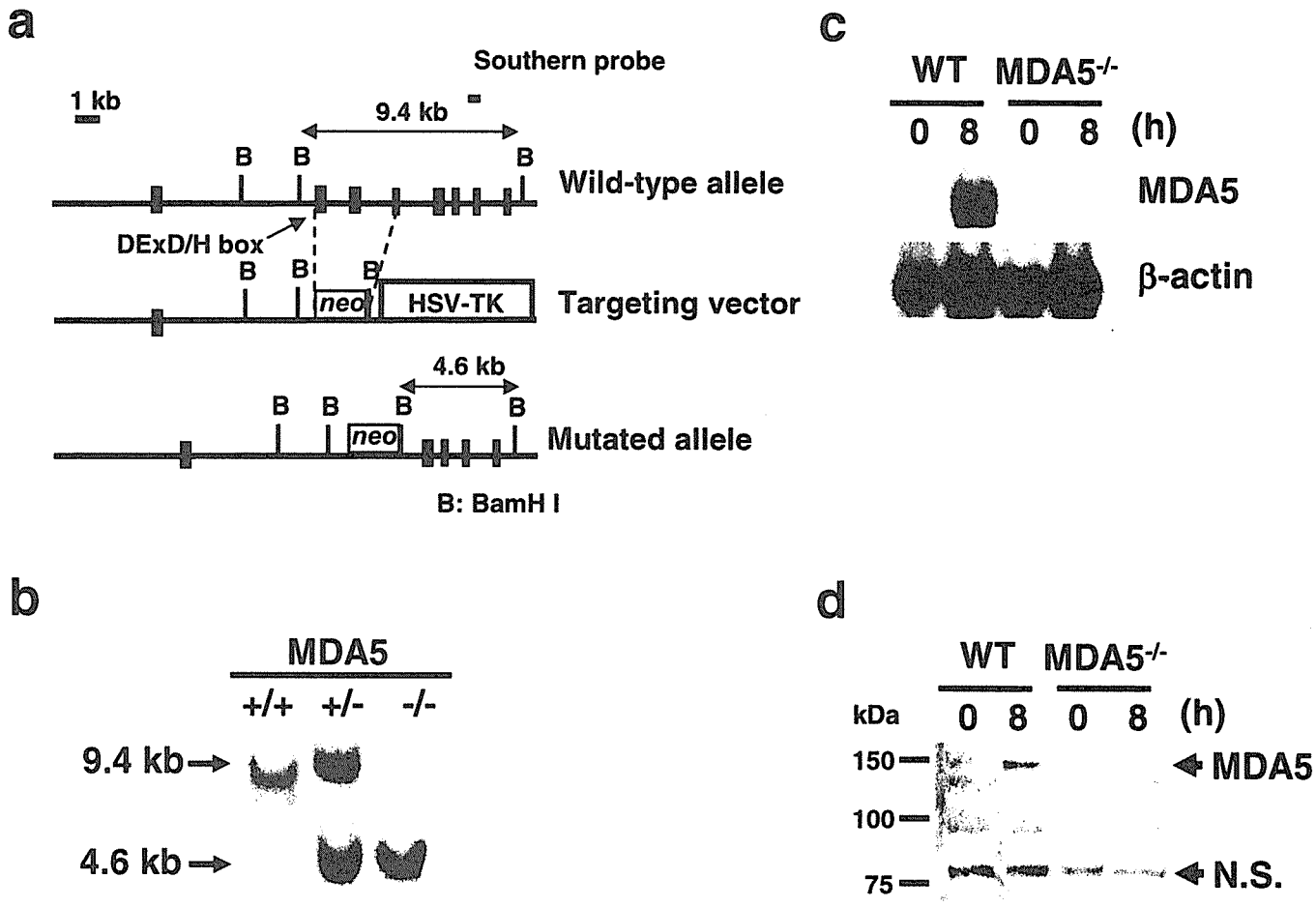

Supplemental Figure 2.